Theoretical Population Biology xxx (xxxx) xxx

Contents lists available at ScienceDirect

Theoretical Population Biology

journal homepage: www.elsevier.com/locate/tpb

PRDM9 and the evolution of recombination hotspots

Francisco Úbeda *, Timothy W. Russell, Vincent A.A. Jansen

School of Biological Sciences, Royal Holloway University of London, Egham, Surrey, TW20 0EX, UK

ARTICLE INFO

Article history:
Received 15 August 2018
Available online xxxx

Keywords:
Recombination hotspot paradox
PRDM9
Population genetics
Gene conversion
Viability selection
Heteroclinic cycles

ABSTRACT

Recombination in mammals is not uniformly distributed along the chromosome but concentrated in small regions known as recombination hotspots. Recombination starts with the double-strand break of a chromosomal sequence and results in the transmission of the sequence that does not break (preventing recombination) more often than the sequence that breaks (allowing recombination). Thus recombination itself renders individual recombination hotspots inactive and over time should drive them to extinction in the genome. Empirical evidence shows that individual recombination hotspots die but, far from being driven to extinction, they are abundant in the genome: a contradiction referred to as the Recombination Hotspot Paradox. What saves recombination hotspots from extinction? The current answer relies in the formation of new recombination hotspots in new genomic sites driven by viability selection in favor of recombination. Here we formulate a population genetics model that incorporates the molecular mechanism initiating recombination in mammals (PRDM9-like genes), to provide an alternative solution to the paradox. We find that weak selection allows individual recombination hotspots to become inactive (die) while saving them from extinction in the genome by driving their re-activation (resurrection). Our model shows that when selection for recombination is weak, the introduction of rare variants causes recombination sites to oscillate between hot and cold phenotypes with a recombination hotspot dying only to come back. Counter-intuitively, we find that low viability selection leaves a hard selective sweep signature in the genome, with the selective sweep at the recombination hotspot being the hardest when viability selection is the lowest. Our model can help to understand the rapid evolution of PRDM9, the co-existence of two types of hotspots, the life expectancy of hotspots, and the volatility of the recombinational landscape (with hotspots rarely being shared between closely related species).

© 2019 Elsevier Inc. All rights reserved.

1. Introduction

The distribution of recombination in the genome – and thus crossover events – is key to our understanding of the molecular mechanisms controlling recombination, the role of recombination on evolution, and the implementation of tests linking genetic markers with human disease (genome-wide association studies) (Boulton et al., 1997; Hey, 2004; Rosenberg et al., 2010). In many mammals, recombination is not uniformly distributed in the genome but concentrated in small chromosomal regions – known as recombination hotspots – where recombination is ten to a thousand times more frequent than the genome's average (Lichten and Goldman, 1995; Petes, 2001; Myers et al., 2005; Paigen and Petkov, 2010). While recombination hotspots are abundant in the mammalian genome (for example, in the human genome there are more than twenty five thousand), their mere existence is paradoxical and their life cycle is not fully understood (Boulton et al., 1997; Pineda-Krch and Redfield, 2005; Myers et al., 2005).

Recombination is initiated by a double-strand break (DSB) and may result in the conversion of the allelic sequence that breaks (active allele, enabling recombination) into the allelic sequence that does not break (inactive allele, disabling recombination) (Lichten and Goldman, 1995; Petes, 2001). The conversion of the allele that enables recombination into the one that disables recombination should be faster in genomic regions where recombination is higher (recombination hotspots). As a result individual recombination hotspots should become inactive (this process is often referred as the death of a hotspot; Coop and Myers, 2007) and, over evolutionary time, recombination hotspots should disappear from the genome (Boulton et al., 1997; Pineda-Krch and Redfield, 2005). Empirical work shows that individual recombination hotspots die (Ptak et al., 2004, 2005; Winckler et al., 2005; Coop et al., 2008; Myers et al., 2010; Stevison et al., 2015) but, despite their self-destructive nature, recombination hotspots are abundant in the mammalian genome (Myers et al., 2005; Baudat et al., 2013), thus posing the Recombination Hotspot Paradox (Boulton et al., 1997; Pineda-Krch and Redfield, 2005): what saves recombination hotspots from extinction?

Due to its molecular, evolutionary and medical implications the Recombination Hotspot Paradox has received much attention.

* Corresponding author.
E-mail address: f.ubeda@rhul.ac.uk (F. Úbeda).

https://doi.org/10.1016/j.tpb.2018.12.005
0040-5809/© 2019 Elsevier Inc. All rights reserved.

Initial work aimed to test whether the known beneficial effects of recombination – in particular how recombination may favor proper chromosomal segregation during meiosis; thus avoiding the formation of aneuploidy gametes (Hassold et al., 2000; Louis and Borts, 2003; Brick et al., 2012; Alves et al., 2017) – can solve the paradox (Boulton et al., 1997; Pineda-Krch and Redfield, 2005; Calabrese, 2007; Peters, 2008). These mathematical models found that the strength of viability selection needed to maintain active alleles at recombination hotspots over evolutionary time was too high to be realistic (Boulton et al., 1997; Pineda-Krch and Redfield, 2005; Calabrese, 2007; Peters, 2008). Furthermore, in these models when viability selection prevents the extinction of hotspots in the genome, it does so by preventing the death of individual hotspots, which is contrary to empirical observations (Ptak et al., 2004, 2005; Winckler et al., 2005; Coop et al., 2008; Myers et al., 2010; Stevison et al., 2015). Therefore, far from providing solutions to the Recombination Hotspot Paradox, previous work demonstrates that the paradox is well grounded.

Recent advances in our understanding of the molecular mechanisms initiating recombination include the identification of gene PRDM9 in humans (and many mammals) coding for protein PRDM9 that may bind a specific sequence at a target recombination hotspot (Myers et al., 2010; Baudat et al., 2010). Binding specificity between PRDM9 and its target site is required for the initiation of recombination (Myers et al., 2010; Baudat et al., 2010). This finding led to the verbal argument that when a target site has its binding motif (active allele) replaced by the non-binding motif (inactive allele) due to biased gene conversion, a mutant PRDM9 could create a new target site by coding for a new binding motif (Myers et al., 2010; Baudat et al., 2010). Natural selection would thus favor this rare mutant PRDM9 as long as recombination is advantageous for the individual (Myers et al., 2010; Baudat et al., 2010). Lacking a mathematical model to back this claim, it remained unclear whether selection would favor such mutant to the extent of allowing the formation (henceforth birth) of new recombination hotspots before an inactive allele arose. Furthermore, would the strength of selection required for the birth of new hotspots be too high to be realistic?

Úbeda and Wilkins (2011) modeled a trans-acting modifier locus with binding specificity – like PRDM9 – showing that, for a strength of selection lower than in previous models, new recombination hotspots can be born at new target sites, while existing recombination hotspots die (Úbeda and Wilkins, 2011). These findings were consistent with empirical observations regarding the persistence of recombination hotspots in the genome in spite of the death of individual recombination hotspots (Úbeda and Wilkins, 2011). The Red Queen hypothesis of recombination hotspots evolution refers to the balance between death and birth of new hotspots driven by conversion and viability selection (Úbeda and Wilkins, 2011), and is the prevailing explanation to the recombination hotspots paradox (Lesecque et al., 2014; Latrille et al., 2017).

In many respects, however, the Red Queen hypothesis needs further theoretical investigation (Latrille et al., 2017). One of these key theoretical aspects is the role of viability selection in maintaining recombination hotspots, and the evolution of PRDM9 and target sequences (Ségurel et al., 2011; Latrille et al., 2017). Recent models include variables that mask the effect of selection; for example drift, recurrent mutation, and multiple locus targets (Úbeda and Wilkins, 2011; Latrille et al., 2017). While the introduction of these variables is justified to make the models more realistic, they complicate our understanding of the interplay between the key variables of these models, namely conversion and selection.

Here we formulate a population genetics model aimed to explore the interplay between conversion and selection in the resolution of the Recombination Hotspot Paradox. We start by considering an infinite population, without recurrent mutation and with a single target locus, to eliminate the above mentioned confounding variables. We build on the insight gained from this minimal model to interpret the results of an extended model with a finite population and recurrent mutation. In doing so, we find an alternative solution to the Recombination Hotspot Paradox, one that does not require the formation of new hotspots but relies on existing hotspots. Counter-intuitively, in our novel solution, it is low viability selection regimes that allow the persistence of recombination hotspots in spite of the death of individual ones (contrary to previous models) (Boulton et al., 1997; Pineda-Krch and Redfield, 2005; Calabrese, 2007; Peters, 2008; Latrille et al., 2017). Furthermore, sometimes, low viability selection accelerates the turnover of hotspots. We also find that viability selection can maintain polymorphisms at the PRDM9 and target loci. We apply these findings to explore the molecular signatures of selection in PRDM9 and target loci and consider their implications for genome-wide association studies.

2. Methods

2.1. Two-locus n-alleles model

We follow the classic Wright–Fisher population genetics framework (Wright, 1969; Bürger, 2000) to formulate a discrete time mathematical model of an infinite population of diploid individuals carrying two loci with an arbitrary number of alleles in each locus.

This model represents the interaction between a gene (PRDM9-like) producing a protein that binds a specific motif at a target recombination site (Fig. 1), as it is observed in humans and many mammals (Myers et al., 2010; Baudat et al., 2010, 2013). The modifier locus A may carry alleles $A_1, A_2, \ldots, A_I$ each encoding a protein that attempts to bind a motif at a target locus B. Locus B may carry alleles $B_1, B_2, \ldots, B_K$ each corresponding to a base pair motif that the protein produced by locus A may attempt to bind. In each generation, both modifier alleles in each diploid individual show the same level of expression producing proteins that have equal probability of binding the two target motifs (Fig. 1). Therefore, in an individual with genotype $\frac{A_iB_k}{A_jB_l}$, the probability that a protein produced by alleles A_i or A_j attempts to bind the motif of alleles B_k or B_l is $\frac{1}{4}$ (Fig. 1). The binding attempt of the protein A_i to the motif B_k results in binding and a double-strand break of allele B_k with probability $b_{i,k}$. However, the binding attempt may result in failure to bind and lack of any double-strand break with probability $1 - b_{i,k}$ (where $0 < b_{i,k} < 1$) (Fig. 1).

A double-strand break initiates recombination and the chromatid that breaks is often repaired using its homologous chromatid as a template (Lichten and Goldman, 1995; Petes, 2001) (Fig. 1). During the repair process there might be a crossover event in or near the target locus with probability r and none with probability $1-r$ (where $0 < r < 1$) (Lichten and Goldman, 1995; Petes, 2001) (Fig. 1). In our model, we assume that a crossover event between the modifier and target loci requires a double-strand break at the target locus. However, if the modifier and target loci are far apart in the same chromosome or in separate chromosomes, a crossover event between these loci may not require a double-strand break. Whether a crossover event between the modifier and target loci require a double-strand break at the target locus or not does not change any of the qualitative results of our model (see the Supplemental Material for a formulation of this model and Fig. 2 for a summary of the results). During the repair process there might also be conversion of the allelic motif that breaks into the allelic motif that does not break with probability c and restoration to the allelic motif that breaks with probability $1-c$ (where $0 < c < 1$) (Szostak et al., 1983; Sun et al., 1991; Lichten and Goldman, 1995; Petes, 2001) (Fig. 1). Typically c takes the value $\frac{1}{2}$ (Szostak et al., 1983; Sun et al., 1991; Lichten and Goldman, 1995; Petes, 2001). Notice

Please cite this article as: F. Úbeda, T.W. Russell and V.A.A. Jansen, PRDM9 and the evolution of recombination hotspots. Theoretical Population Biology (2019), https://doi.org/10.1016/j.tpb.2018.12.005.

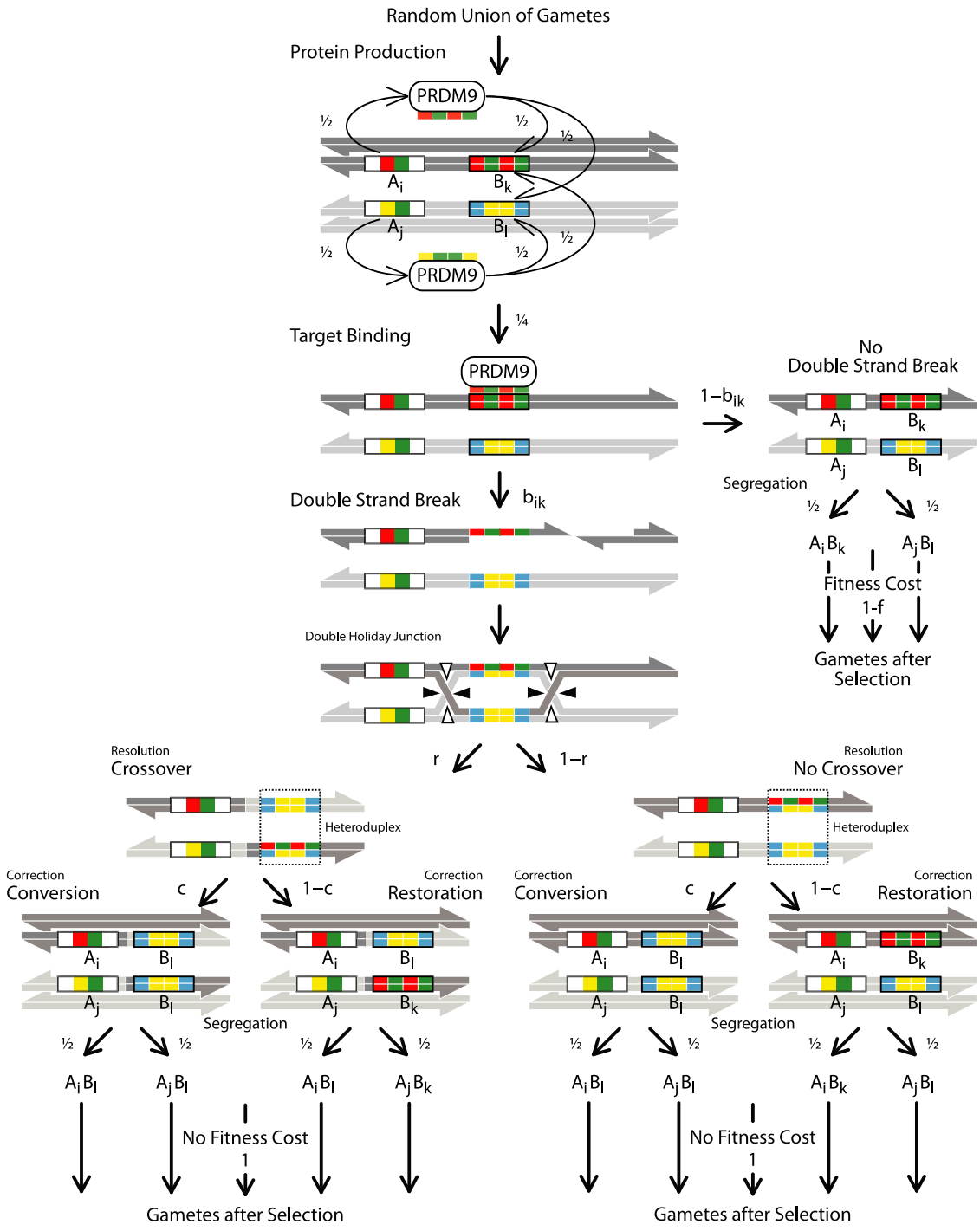

Fig. 1. *Model for recombination initiated by specificity of the double strand break.* Summary of the sequence of events modeled. We start with the production of a PRDM9-like protein with a recognition sequence that may match the target motif (same color sequence in recognition and motif) or not (different color sequence in recognition and motif). If protein and target bind, we follow the canonical DSB repair model for the initiation of recombination (Szostak et al., 1983; Sun et al., 1991). Once recombination (including crossover and conversion effects) has been completed, we model Mendelian segregation of haplotypes with no fitness cost. If protein and target do not bind, there is no recombination and we model Mendelian segregation of haplotypes with a fitness cost. Notice that sister chromatids are represented at the beginning and end of the figure but are omitted from the middle part for clarity. (For interpretation of the references to color in this figure legend, the reader is referred to the web version of this article.)

that biased gene conversion results in the over-transmission of the allele that is less likely to break (Boulton et al., 1997; Petes, 2001) (Figure 1).

Recombination ends up with Mendelian segregation of alleles into gametes. Following previous models (Boulton et al., 1997; Pineda-Krch and Redfield, 2005; Peters, 2008; Úbeda and Wilkins, 2011; Latrille et al., 2017), we assume that individuals undergoing recombination at the target locus have proper chromosomal segregation and do not suffer any fitness cost, while individuals that do not undergo recombination at the target locus have defective chromosomal segregation producing aneuploid (non-viable) gametes with probability f (where $0 < f < 1$) (Fig. 1). Therefore, the fitness of individuals experiencing a recombination event is 1 but the fitness of individuals not experiencing a recombination event is

Please cite this article as: F. Úbeda, T.W. Russell and V.A.A. Jansen, PRDM9 and the evolution of recombination hotspots. Theoretical Population Biology (2019), https://doi.org/10.1016/j.tpb.2018.12.005.

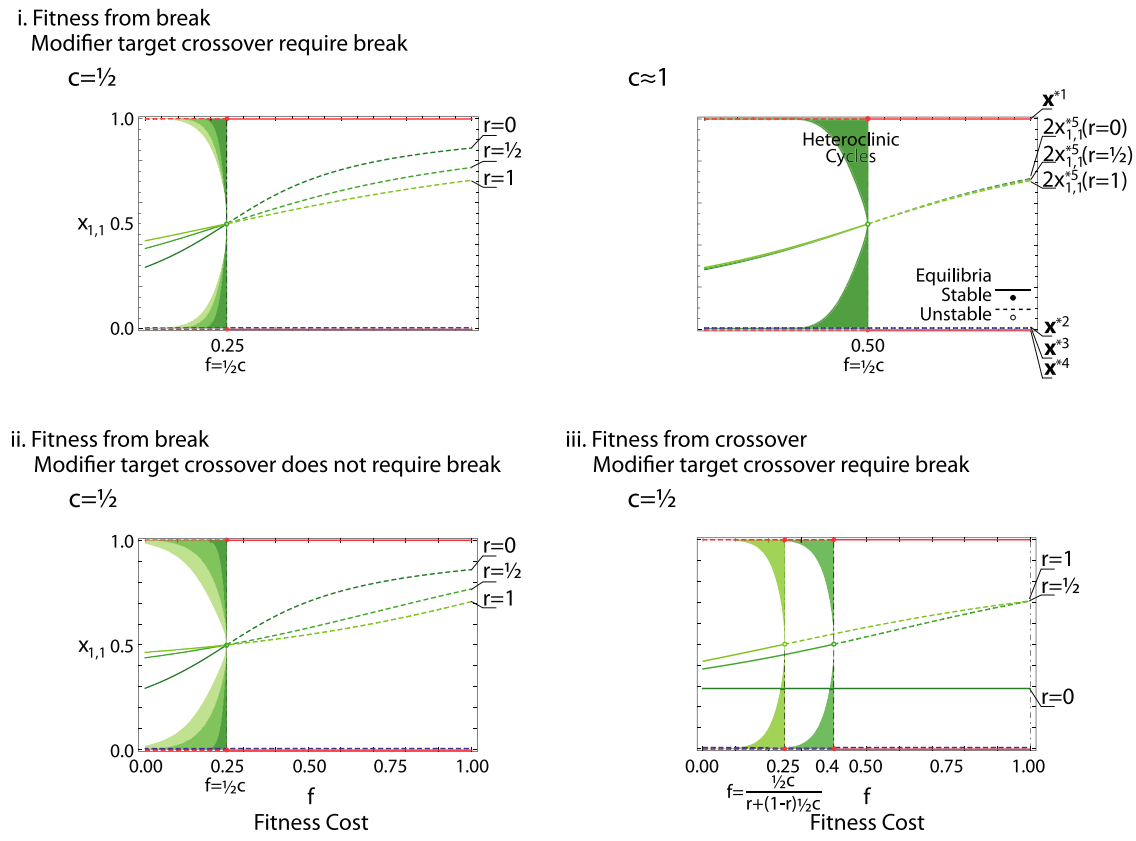

Fig. 2. *Equilibria and heteroclinic cycle.* Summary of the equilibria with biological meaning, their stability and the basin of attraction of the heteroclinic cycle for three alternative models. Each panel corresponds to a different model given a specific value of the conversion rate c. Shades of green correspond to different values of the crossover rate $r = \{0, \frac{1}{2}, 1\}$ (with darker green corresponding to no-crossover $r = 0$). For each pair of values (c, r), the equilibrium frequency of haplotype $x^*_{1,1}$ is plotted as a function of the fitness cost f. Red lines depict corner equilibria $\mathbf{x}^{*1}$ and $\mathbf{x}^{*4}$ corresponding to the fixation of recombination enabling haplotypes (notice that these are independent of the values of c and r). Blue lines depict corner equilibria $\mathbf{x}^{*2}$ and $\mathbf{x}^{*3}$ corresponding to the fixation of recombination disabling haplotypes (notice that these are independent of the values of c and r). Green lines depict twice $x^*_{1,1}$ of internal equilibrium $\mathbf{x}^{*5}$ corresponding to a polymorphism between recombination enabling and disabling haplotypes. Continuous lines depict stable equilibria while dashed lines depict unstable equilibria. The green colored area corresponds to the region in the space formed by the initial frequencies $(x^0_{1,1}, 0, 0, 1 - x^0_{1,1})$ and the fitness cost f where the system tends to the heteroclinic cycle $(\ldots \mathbf{x}^{*1} \rightarrow \mathbf{x}^{*2} \rightarrow \mathbf{x}^{*4} \rightarrow \mathbf{x}^{*3} \rightarrow \mathbf{x}^{*1} \ldots)$ as opposed to the internal equilibrium $\mathbf{x}^{*5}$. Shades of green correspond to different values of the crossover rate $r = \{0, \frac{1}{2}, 1\}$ (with darker green corresponding to no-crossover $r = 0$). (i) The first panel corresponds to the case presented in the main text where selection is determined by double-strand breaks, and crossover events between the PRDM-9 and its target loci require a double-strand break at the target locus. (ii) The second panel corresponds to the case where selection is determined by crossover events, and crossover events between the PRDM-9 and its target loci require a double-strand break at the target locus. (iii) The third panel corresponds to the case where selection is determined by double-strand breaks, and crossover events between the PRDM-9 and its target loci do not require a double-strand break at the target locus. (For interpretation of the references to color in this figure legend, the reader is referred to the web version of this article.)

$1-f$ (Fig. 1). Proper chromosomal segregation, however, often requires a crossover event rather than a recombination event (Baker et al., 1976; Koehler et al., 1996; Hassold and Hunt, 2001; Louis and Borts, 2003; Brick et al., 2012; Alves et al., 2017). Whether it is a crossover or a recombination event that determine the probability of proper chromosomal segregation does not change any of the qualitative results of our model (see the Supplemental Material for a formulation of this model and Fig. 2 for a summary of the results).

Let $x_{i,k}$ be the frequency of haplotype A_iB_k in gametes. Notice that $0 \leq x_{i,k} \leq 1$ and $\sum_{i,k} x_{i,k} = 1$. Random union of gametes results in an embryo with genotype $\frac{A_iB_k}{A_jB_l}$ with frequency $x_{i,k}x_{j,l}$. The probability that this embryo reaches adulthood is independent of its genotype, but its genotype determines the outcome of meiosis in adults. In particular, the probability that during meiosis the protein produced by the modifier locus breaks targets B_k and B_l are $\bar{b}_{ij,k} = \frac{1}{2}(b_{i,k} + b_{j,k})$ and $\bar{b}_{ij,l} = \frac{1}{2}(b_{i,l} + b_{j,l})$ respectively, and the probability that it breaks one of the targets is $\bar{\bar{b}}_{ij,kl} = \frac{1}{2}(\bar{b}_{ij,k} + \bar{b}_{ij,l})$. The probability that during meiosis a double-strand break is followed by a crossover event between alleles at locus A and B is r, and the probability that the motif that breaks is converted into the motif that does not break is c. Recombination at the target locus is followed by correct Mendelian segregation of haplotypes into gametes but in the absence of recombination segregation of haplotypes is incorrect with probability f. Haplotype segregation brings us back to the beginning of our census.

The frequency of haplotype A_iB_k in gametes in the next generation is:

$$\begin{aligned} x'_{i,k} = \frac{1}{\bar{w}} \sum_{j,l} \tfrac{1}{2}[(\bar{\bar{b}}_{ij,kl} + (1 - \bar{\bar{b}}_{ij,kl})(1-f))x_{i,k}x_{j,l} \\ - \tfrac{1}{4}c(\bar{b}_{ij,k}x_{i,k}x_{j,l} - \bar{b}_{ij,l}x_{i,l}x_{j,k}) \\ - \tfrac{1}{2}(1-c)r\bar{\bar{b}}_{ij,kl}(x_{i,k}x_{j,l} - x_{i,l}x_{j,k})] \end{aligned} \quad (1)$$

where prime represents the next generation and:

$$\bar{w} = \sum_{i,k}\sum_{j,l} \tfrac{1}{2}[\bar{\bar{b}}_{ij,kl} + (1 - \bar{\bar{b}}_{ij,kl})(1-f)]x_{i,k}x_{j,l} \quad (2)$$

is the population mean fitness. These changes in haplotype frequency underpin changes in the population mean crossover rate at the target locus:

$$\bar{r} = \tfrac{1}{2}r \sum_{i,k}\sum_{j,l} \bar{\bar{b}}_{ij,kl}x_{i,k}x_{j,l} \quad (3)$$

which is the phenotype whose evolution we are interested in.

Please cite this article as: F. Úbeda, T.W. Russell and V.A.A. Jansen, PRDM9 and the evolution of recombination hotspots. Theoretical Population Biology (2019), https://doi.org/10.1016/j.tpb.2018.12.005.

Our model greatly differs from all other attempts to incorporate binding specificity (PRDM9-like genes) into the mechanism of recombination hotspots (Úbeda and Wilkins, 2011; Latrille et al., 2017). Furthermore, previous models relied on simulations for the analysis while we present analytic results (although see Latrille et al. (2017) for a one locus model approximating the frequency of PRDM9-like alleles in an infinite population).

2.2. Two-locus two-allele model

We consider the above model in the particular case when there are two alleles (A_1, A_2) at the modifier locus and two alleles (B_1, B_2) at the only target locus, resulting in four different haplotypes $(A_1B_1, A_1B_2, A_2B_1, A_2B_2)$. Henceforth, we assume that a match between the subscripts of the modifier allele producing the binding protein and the allelic sequence that is the target of this protein results in a double-strand break with probability b (where $0 < b < 1$) and a mismatch between the subscripts prevents a double-strand break. For our modeling purposes this translates into:

$$b_{i,k} = \begin{cases} b & \text{if } i = k \\ 0 & \text{if } i \neq k. \end{cases}$$

Notice that two of these haplotypes (A_1B_1, A_2B_2) correspond to haplotypes producing a protein that matches its own recognition sequence (recombination enabling haplotypes) and the other two (A_1B_2, A_2B_1) correspond to haplotypes producing a protein that does not match its own recognition sequence (recombination disabling haplotypes).

The dynamic system describing the change in frequency over time of each of these haplotypes can be obtained from replacing generic subscripts i and k by specific subscripts 1 and 2 in Eq. (1). The frequency of haplotype A_iB_k in gametes in the next generation is:

$$\begin{aligned}
\bar{w}x'_{1,1} =& (\tfrac{1}{4}b + \tfrac{1}{2}(1-\tfrac{1}{2}b)(1-f) + \tfrac{1}{4}bfx_{1,1} - \tfrac{1}{8}bcx_{1,2})x_{1,1} \\
& - \tfrac{1}{8}b(\tfrac{1}{2}c + (1-c)r)D \\
\bar{w}x'_{1,2} =& (\tfrac{1}{4}b + \tfrac{1}{2}(1-\tfrac{1}{2}b)(1-f) - \tfrac{1}{4}bfx_{1,2} + \tfrac{1}{8}bcx_{1,1})x_{1,2} \\
& + \tfrac{1}{8}b(\tfrac{1}{2}c + (1-c)r)D \\
\bar{w}x'_{2,1} =& (\tfrac{1}{4}b + \tfrac{1}{2}(1-\tfrac{1}{2}b)(1-f) - \tfrac{1}{4}bfx_{2,1} + \tfrac{1}{8}bcx_{2,2})x_{2,1} \\
& + \tfrac{1}{8}b(\tfrac{1}{2}c + (1-c)r)D \\
\bar{w}x'_{2,2} =& (\tfrac{1}{4}b + \tfrac{1}{2}(1-\tfrac{1}{2}b)(1-f) + \tfrac{1}{4}bfx_{2,2} - \tfrac{1}{8}bcx_{2,1})x_{2,2} \\
& - \tfrac{1}{8}b(\tfrac{1}{2}c + (1-c)r)D
\end{aligned} \tag{4}$$

where

$$\bar{w} = \tfrac{1}{4}b + \tfrac{1}{2}(1-\tfrac{1}{2}b)(1-f) + \tfrac{1}{4}bf(x_{1,1}^2 + x_{2,2}^2 - x_{1,2}^2 - x_{2,1}^2) \tag{5}$$

is the population mean fitness and:

$$D = x_{1,1}x_{2,2} - x_{1,2}x_{2,1} \tag{6}$$

is the linkage disequilibrium.

To simplify the analysis, we define parameters α, β, γ, and δ as follows:

$$\begin{aligned}
\bar{w}x'_{i,k} =& \underbrace{(\tfrac{1}{4}b + \tfrac{1}{2}(1-\tfrac{1}{2}b)(1-f)}_{\alpha} \pm \underbrace{\tfrac{1}{4}bf}_{\beta}\, x_{i,k} \pm \underbrace{\tfrac{1}{8}bc}_{\gamma}\, x_{i,l})x_{i,k} \\
& \pm \underbrace{\tfrac{1}{8}b(\tfrac{1}{2}c + (1-c)r)}_{\delta} D
\end{aligned} \tag{7}$$

which allows us to re-write the system of Eqs. (4) as follows:

$$\begin{aligned}
\bar{w}x'_{1,1} =& (\alpha + \beta x_{1,1} - \gamma x_{1,2})x_{1,1} - \delta D \\
\bar{w}x'_{1,2} =& (\alpha - \beta x_{1,2} + \gamma x_{1,1})x_{1,2} + \delta D \\
\bar{w}x'_{2,1} =& (\alpha - \beta x_{2,1} + \gamma x_{2,2})x_{2,1} + \delta D \\
\bar{w}x'_{2,2} =& (\alpha + \beta x_{2,2} - \gamma x_{2,1})x_{2,2} - \delta D
\end{aligned} \tag{8}$$

with population mean fitness:

$$\bar{w} = \alpha + \beta(x_{1,1}^2 - x_{1,2}^2 - x_{2,1}^2 + x_{2,2}^2). \tag{9}$$

Notice that $0 < \alpha, \beta, \gamma, \delta < 1$. This two-locus two-allele model shares some similarities with the well-known symmetric viability model of Karlin et al. (1970) and Bürger (2000), albeit our model is not symmetrical and therefore the results of the symmetric viability model do not carry over.

3. Results

3.1. Equilibria

We apply the equilibrium conditions $(x'_{i,k} = x_{i,k} = x^*_{i,k}$ for all $i, k)$ to system (8) to find five equilibria with biological meaning; where all haplotype frequencies lie between (and including) 0 and 1. Let $\mathbf{x}^{*e} = (x^{*e}_{1,1}, x^{*e}_{1,2}, x^{*e}_{2,1}, x^{*e}_{2,2})$ denote the haplotype frequencies at equilibrium e where e is between one and five.

The first four equilibria correspond to the corners of the three dimensional simplex:

$$\begin{aligned}
\mathbf{x}^{*1} &= (1, 0, 0, 0) \\
\mathbf{x}^{*2} &= (0, 1, 0, 0) \\
\mathbf{x}^{*3} &= (0, 0, 1, 0) \\
\mathbf{x}^{*4} &= (0, 0, 0, 1).
\end{aligned} \tag{10}$$

Notice that equilibria 1 and 4, $\mathbf{x}^{*1}$ and $\mathbf{x}^{*4}$, correspond to the fixation of one of the two recombination enabling haplotypes, $x_{1,1}$ and $x_{2,2}$ respectively. Equilibria 2 and 3, $\mathbf{x}^{*2}$ and $\mathbf{x}^{*3}$, correspond to the fixation of one of the two recombination disabling haplotypes, $x_{1,2}$ and $x_{2,1}$ respectively (Fig. 2).

The last equilibrium can be obtained by noticing some symmetries of our model. In particular, if at any point $x_{1,1} = x_{2,2}$ and $x_{1,2} = x_{2,1}$, this remains so in the future. To see this, notice that if $x_{1,1} = x_{2,2}$ and $x_{1,2} = x_{2,1}$, the difference equations become $x'_{1,1} = x'_{2,2}$ and $x'_{1,2} = x'_{2,1}$ and the changes in $x_{1,1}$ and $x_{1,2}$ are equal to the changes in $x_{2,2}$ and $x_{2,1}$ respectively. Also note that if $x_{1,1} = x_{2,2}$ and $x_{1,2} = x_{2,1}$ and keeping in mind that $x_{1,1} + x_{1,2} + x_{2,1} + x_{2,2} = 1$, we also have that $2x_{1,1} + 2x_{1,2} = 1$ and thus $x_{1,2} = \frac{1}{2} - x_{1,1}$.

The existence of a one dimensional manifold which is invariant in the interior of the state space implies that there is a symmetric equilibrium. The dynamics on this manifold are described by a single difference equation:

$$\bar{w}x'_{1,1} = (\alpha + \beta x_{1,1} - \gamma(\tfrac{1}{2} - x_{1,1}))x_{1,1} - \delta(x_{1,1} - \tfrac{1}{4}) \tag{11}$$

with population mean fitness:

$$\bar{w} = \alpha + 2\beta(x_{1,1} - \tfrac{1}{4}). \tag{12}$$

Applying the equilibrium condition $(x'_{1,1} = x_{1,1} = x^*_{1,1})$ to the previous equation yields the symmetric equilibrium:

$$\begin{aligned}
\mathbf{x}^{*5} &= (x^{*5}_{1,1}, \tfrac{1}{2} - x^{*5}_{1,1}, \tfrac{1}{2} - x^{*5}_{1,1}, x^{*5}_{1,1}) \\
x^{*5}_{1,1} &= \tfrac{1}{4} + \tfrac{1}{4}\tfrac{2\delta - \sqrt{(2\delta)^2 + (\gamma-\beta)^2}}{\gamma - \beta}.
\end{aligned} \tag{13}$$

At this equilibrium, the linkage disequilibrium is:

$$D^* = x^{*5}_{1,1} - \tfrac{1}{4} = \tfrac{1}{4}\tfrac{2\delta - \sqrt{(2\delta)^2 + (\gamma-\beta)^2}}{\gamma - \beta}, \tag{14}$$

and the population mean fitness is:

$$\bar{w}^* = \alpha + 2\beta(x^*_{1,1} - \tfrac{1}{4}) = \alpha + 2\beta D^*. \tag{15}$$

Notice that equilibrium $\mathbf{x}^{*5}$ corresponds to a polymorphism where all haplotypes (recombination enablers and disablers) are preserved.

Please cite this article as: F. Úbeda, T.W. Russell and V.A.A. Jansen, PRDM9 and the evolution of recombination hotspots. Theoretical Population Biology (2019), https://doi.org/10.1016/j.tpb.2018.12.005.

Finally, we can re-write the expression for equilibrium $\mathbf{x}^{*5}$ in terms of the original parameters of our model:

$$x^{*5}_{1,1} = \frac{1}{4} + \frac{1}{4}\frac{\frac{1}{2}c+(1-c)r-\sqrt{(\frac{1}{2}c+(1-c)r)^2+(\frac{1}{2}c-f)^2}}{\frac{1}{2}c-f} \tag{16}$$

3.2. Stability

The stability of an equilibrium $\mathbf{x}^{*e}$ of a map $\mathbf{x}' = \mathbf{g}(\mathbf{x})$ is determined by studying the eigenvalues λ^e of the Jacobian matrix $\mathbf{J}$ of the map evaluated at the equilibrium, that is $\mathbf{J}|_{\mathbf{x}=\mathbf{x}^{*e}}$. For brevity, we will refer to the eigenvalues λ^e_i as the eigenvalues of equilibrium $\mathbf{x}^{*e}$. If the modulus of all eigenvalues of equilibrium $\mathbf{x}^{*e}$ is less than one ($|\lambda^e_i| < 1$ for all $i = 1, \ldots, n$), the equilibrium is linearly stable (where $|z|$ denotes the modulus of a number z that may have real $\mathrm{Re}(z)$ and imaginary $\mathrm{Im}(z)$ components and is defined as $|z| = \sqrt{\mathrm{Re}(z)^2 + \mathrm{Im}(z)^2}$). If the modulus of at least one eigenvalue of equilibrium $\mathbf{x}^{*e}$ is greater than one ($|\lambda^e_i| > 1$ for any $i = 1, \ldots, n$), the equilibrium is linearly unstable.

The specifics of our model simplify the calculation of the Jacobian at equilibrium. In particular, our model describes changes in haplotype frequencies. To ensure that all frequencies add up to one at all times, the changes in frequency are normalized and the system is of the form:

$$\mathbf{x}' = \frac{\mathbf{g}(\mathbf{x})}{\bar{w}(\mathbf{x})} \tag{17}$$

where $\bar{w}(\mathbf{x}) = \mathbf{1}^T\mathbf{g}(\mathbf{x})$, $\mathbf{1}$ is a vector with all entries equal to one, and subscript T is the transpose operator. The Jacobian of this system is:

$$\mathbf{J} = D_x\frac{\mathbf{g}(\mathbf{x})}{\bar{w}(\mathbf{x})} = \frac{D_x\mathbf{g}(\mathbf{x})}{\bar{w}(\mathbf{x})} - \frac{\mathbf{g}(\mathbf{x})}{\bar{w}(\mathbf{x})}\frac{\mathbf{1}^T D_x\mathbf{g}(\mathbf{x})}{\bar{w}(\mathbf{x})}, \tag{18}$$

where D_x is the total derivative with respect to x. Evaluated at equilibrium $\mathbf{x}^*$ the Jacobian reduces to:

$$\mathbf{J}|_{\mathbf{x}=\mathbf{x}^*} = \frac{1}{\bar{w}(\mathbf{x}^*)}(\mathbf{I} - \mathbf{x}^*\mathbf{1}^T)\, D_x\mathbf{g}(\mathbf{x})|_{\mathbf{x}=\mathbf{x}^*}\,. \tag{19}$$

where $\mathbf{I}$ is the identity matrix.

3.2.1. Corner equilibria

The eigenvalues of corner equilibria $\mathbf{x}^{*1}$ and $\mathbf{x}^{*4}$ are equal and given by:

$$\{\lambda^1_1, \lambda^1_2, \lambda^1_3, \lambda^1_4\} = \{\lambda^4_1, \lambda^4_2, \lambda^4_3, \lambda^4_4\} = \left(0, \tfrac{\alpha}{\alpha+\beta}, \tfrac{\alpha+\gamma}{\alpha+\beta}, \tfrac{\alpha-\delta}{\alpha+\beta}\right). \tag{20}$$

All eigenvalues of corner equilibrium $\mathbf{x}^{*1}$ are real numbers, and $\mathbf{x}^{*1}$ is stable if all λ^1_{1-4} lie between 1 and -1.

1. Condition $-1 < \lambda^1_2 < 1$ is always satisfied.
2. Condition $-1 < \lambda^1_3 < 1$ implies the satisfaction of:
   i. $\lambda^1_3 < 1$ which requires that $\beta > \gamma$.
   ii. $\lambda^1_3 > -1$ which is always satisfied.
3. Condition $-1 < \lambda^1_4 < 1$ implies the satisfaction of:
   i. $\lambda^1_4 < 1$ which is always satisfied.
   ii. $\lambda^1_4 > -1$ which requires that $2\alpha + \beta - \delta > 0$ which is always satisfied for the original parameters of our model.

To summarize, corner equilibria $\mathbf{x}^{*1}$ and $\mathbf{x}^{*4}$ are stable ($-1 < \lambda^1_{2-4} < 1$) if $\beta > \gamma$ ($f > \frac{1}{2}c$ in terms of the original parameters) but unstable (saddles) ($-1 < \lambda^1_{2,4} < 1$ but $\lambda^1_3 > 1$) if $\beta < \gamma$ ($f < \frac{1}{2}c$) (see Table 1 and Fig. 2).

The eigenvalues of corner equilibria $\mathbf{x}^{*2}$ and $\mathbf{x}^{*3}$ are equal and given by:

$$\{\lambda^2_1, \lambda^2_2, \lambda^2_3, \lambda^2_4\} = \{\lambda^3_1, \lambda^3_2, \lambda^3_3, \lambda^3_4\} = \left(0, \tfrac{\alpha}{\alpha-\beta}, \tfrac{\alpha-\gamma}{\alpha-\beta}, \tfrac{\alpha-\delta}{\alpha-\beta}\right). \tag{21}$$

All eigenvalues of corner equilibrium $\mathbf{x}^{*2}$ are real numbers, and $\mathbf{x}^{*2}$ is stable if all λ^2_{1-4} lie between 1 and -1.

1. Condition $-1 < \lambda^2_2 < 1$ implies the satisfaction of:
   i. $\lambda^2_2 < 1$ which is never satisfied.
   ii. $\lambda^2_2 > -1$ which is always satisfied.
2. Condition $-1 < \lambda^2_3 < 1$ implies the satisfaction of:
   i. $\lambda^2_3 < 1$ which requires that $\beta < \gamma$.
   ii. $\lambda^2_3 > -1$ which is always satisfied for the original parameters of our model.

To summarize, corner equilibria $\mathbf{x}^{*2}$ and $\mathbf{x}^{*3}$ are unstable ($\lambda^2_2 > 1$). If $\beta < \gamma$ ($f < \frac{1}{2}c$) these equilibria are saddles ($\lambda^2_2 > 1$ but $-1 < \lambda^2_3 < 1$) (see Table 1 and Fig. 2).

3.2.2. Heteroclinic orbit

Here we show the existence of a heteroclinic orbit between the corner equilibria in our state space: $\ldots\mathbf{x}^{*1} \to \mathbf{x}^{*2} \to \mathbf{x}^{*4} \to \mathbf{x}^{*3} \to \mathbf{x}^{*1}\ldots$. To do so, we need to show that the subspaces in which the heteroclinic orbit travels are invariant. A set, $C \subseteq \mathbb{R}^n$, is an invariant set with respect to the map $x' = g(x)$ if, for every orbit ϕ it is true that $\phi_t(x) \in C \implies \phi_\tau(x) \in C$ for all $\tau > t$ where $t, \tau \in \mathbb{N}_+$. The subspaces in which our heteroclinic orbit travels are described by the lines joining each of the corners of our simplex, namely: $(x_{1,1}, 1-x_{1,1}, 0, 0)$, $(0, x_{1,2}, 0, 1-x_{1,2})$, $(0, 0, 1-x_{2,2}, x_{2,2})$, $(1-x_{2,1}, 0, x_{2,1}, 0)$. Our system can be written in the form:

$$\bar{w}x'_{i,k} = (\alpha + \epsilon\beta x_{i,k} - \epsilon\gamma x_{i,l})x_{i,k} - \epsilon\delta(x_{i,k}x_{j,l} - x_{i,l}x_{j,k}), \tag{22}$$

where $\epsilon = 1$ for $(i,k) = (1,1)$ and $(2,2)$, and $\epsilon = -1$ for $(i,k) = (1,2)$ and $(2,1)$. From the system written in this form, it is easy to see that if $x_{i,k} = 0$ and $x_{i,l} = 0$ or $x_{j,k} = 0$ for $(i,k,j,l) \in 1,2$ then $x'_{i,k} = 0$. In particular for the heteroclinic orbit we consider, either when $x_{2,2} = 0$ then $x_{2,1} = 0$ and $x'_{2,2} = 0$, when $x_{2,1} = 0$ then $x_{1,1} = 0$ and $x'_{2,1} = 0$, when $x_{1,1} = 0$ then $x_{1,2} = 0$ and $x'_{1,1} = 0$, and when $x_{1,2} = 0$ then $x_{2,2} = 0$ and $x'_{1,2} = 0$. This means that any subspace where $x_{i,k} = 0$ and $x_{i,l} = 0$ or $x_{j,k} = 0$ is invariant and thus all subspaces considered in our system are invariants.

When $\beta < \gamma$ ($f < \frac{1}{2}c$ in terms of the original parameters) all corner equilibria are saddles with one incoming and one outgoing eigenvector situated within the lines connecting the corner equilibria. Under the action of our system, the invariant subspaces have orbits which tend always away from one saddle equilibrium and towards another saddle equilibrium, thus implying the existence of a heteroclinic orbit. When $\beta < \gamma$, this heteroclinic orbit is stable (Russell et al., 2019).

3.2.3. Internal equilibrium

Calculating the eigenvalues of the internal equilibrium $\mathbf{x}^{*5}$ using the original Jacobian matrix in (19) leads to intractable results. To attain eigenvalues that are tractable, we transform the vector $\mathbf{x}$ into the vector $\mathbf{y}$ using the linear transformation $\mathbf{y} = \mathbf{M}\mathbf{x}$ where:

$$\mathbf{M} = \begin{bmatrix} 1 & 1 & 1 & 1 \\ 1 & -1 & -1 & 1 \\ 1 & 1 & 0 & 0 \\ 1 & 0 & 1 & 0 \end{bmatrix}. \tag{23}$$

The dynamics in the vicinity of the equilibrium for the transformed variables are:

$$\mathbf{y}' = \mathbf{M}\mathbf{x}' = \mathbf{M}\mathbf{J}\mathbf{x} = \mathbf{M}\mathbf{J}\mathbf{M}^{-1}\mathbf{y}, \tag{24}$$

Table 1
Stability. The *eigenvalue* column contains the eigenvalues corresponding to each equilibrium with biological meaning ($\mathbf{x}^{*1-5}$). The *stability* column summarizes the analysis of the stability of each equilibrium using their eigenvalues. This analysis shows that the stability of all equilibria is determined by a single condition, namely whether $\beta > \gamma$ or not.

Equilibria	Eigenvalues	Stability: $\beta > \gamma$	Stability: $\beta < \gamma$
$\mathbf{x}^{*1} = (1,0,0,0)$ $\mathbf{x}^{*4} = (0,0,0,1)$	$\lambda_1^{1,4} = 0$ $\lambda_2^{1,4} = \frac{\alpha}{\alpha+\beta}$ $\lambda_3^{1,4} = \frac{\alpha+\gamma}{\alpha+\beta}$ $\lambda_4^{1,4} = \frac{\alpha-\delta}{\alpha+\beta}$	$\lambda_i^{1,4}$ **real** $-1 < \lambda_{2,3,4}^{1,4} < 1$ **stable**	$\lambda_i^{1,4}$ **real** $-1 < \lambda_{2,4}^{1,4} < 1$ $\lambda_3^{1,4} > 1$ **unstable** (saddle)
$\mathbf{x}^{*2} = (0,1,0,0)$ $\mathbf{x}^{*3} = (0,0,1,0)$	$\lambda_1^{2,3} = 0$ $\lambda_2^{2,3} = \frac{\alpha}{\alpha-\beta}$ $\lambda_3^{2,3} = \frac{\alpha-\gamma}{\alpha-\beta}$ $\lambda_4^{2,3} = \frac{\alpha-\delta}{\alpha-\beta}$	$\lambda_i^{2,3}$ **real** $\lambda_{2,3}^{2,3} > 1$ **unstable**	$\lambda_i^{2,3}$ **real** $-1 < \lambda_3^{2,3} < 1$ $\lambda_2^{2,3} > 1$ **unstable** (saddle)
$\mathbf{x}^{*5}$	$\lambda_1^5 = 0$ $\lambda_2^5 = 1 + \frac{\gamma D^* + \sqrt{\frac{1}{4}\beta(\beta-\gamma)+(D^*\gamma)^2}}{\bar{w}^*}$ $\lambda_3^5 = 1 + \frac{\gamma D^* - \sqrt{\frac{1}{4}\beta(\beta-\gamma)+(D^*\gamma)^2}}{\bar{w}^*}$ $\lambda_4^5 = 1 - \frac{\delta+2D^*(\beta-\gamma)}{\bar{w}^*}$	λ_i^5 **real** $-1 < \lambda_{3,4}^5 < 1$ $\lambda_2^5 > 1$ **unstable** (saddle)	$\lambda_{2,3}^5$ **imaginary** $-1 < \lambda_4^5 < 1$ $\lvert\lambda_{2,3}^5\rvert < 1$ **stable**

$$\mathbf{MJM}^{-1} = \mathbf{M}\tfrac{1}{\bar{w}^*}(\mathbf{I} - \mathbf{x}^*\mathbf{1}^T)\, D_x\mathbf{g}(\mathbf{x})|_{\mathbf{x}=\mathbf{x}^*}\, \mathbf{M}^{-1} = \begin{bmatrix} 0 & 0 & 0 & 0 \\ \frac{\beta-\gamma-8D^*(\bar{w}^*+\delta)}{2\bar{w}^*} & -\frac{4D^*(\beta-\gamma)-2(\bar{w}^*-\delta)}{2\bar{w}^*} & 0 & 0 \\ -\frac{\bar{w}^*+\frac{1}{2}\beta}{2\bar{w}^*} & 0 & 1 & \frac{\beta}{2\bar{w}^*} \\ -\frac{\frac{1}{2}(\beta-\gamma)+2D^*+\bar{w}^*}{2\bar{w}^*} & 0 & \frac{\beta-\gamma}{2\bar{w}^*} & \frac{4D^*\gamma+2\bar{w}^*}{2\bar{w}^*} \end{bmatrix}. \quad (25)$$

Box I.

where the matrix $\mathbf{MJM}^{-1}$ is given in Box I.

The eigenvalues of the transformed matrix $\mathbf{MJM}^{-1}$ are equivalent to the eigenvalues of the original matrix $\mathbf{J}$ but they are easier to find. In particular, the eigenvalues of matrix $\mathbf{MJM}^{-1}$ are:

$$\{\lambda_1^5, \lambda_2^5, \lambda_3^5, \lambda_4^5\} = \left(0, 1 + \tfrac{\gamma D^* + \sqrt{\Delta^*}}{\bar{w}^*}, 1 + \tfrac{\gamma D^* - \sqrt{\Delta^*}}{\bar{w}^*}, \times\ 1 - \tfrac{\delta + 2D^*(\beta-\gamma)}{\bar{w}^*}\right) \quad (26)$$

where $\Delta^* = (\gamma D^*)^2 + \frac{1}{4}\beta(\beta-\gamma)$.

The eigenvalues of internal equilibrium $\mathbf{x}^{*5}$ can be either real or imaginary numbers.

1. Stability conditions derived from the second and third eigenvalues $\lambda_{2,3}^5$.

   (a) Eigenvalues $\lambda_{2,3}^5$ are real numbers when $\Delta^* > 0$. If $\beta > \gamma$, the later condition is always satisfied, eigenvalues $\lambda_{2,3}^5$ are real numbers, and the stability of the internal equilibrium requires that $-1 < \lambda_{2,3}^5 < 1$. This requirement implies the satisfaction of four conditions:

   i. Condition $\lambda_2^5 < 1$ requires that $\gamma D^* + \sqrt{\Delta^*} < 0$ which is never satisfied.
   ii. Condition $\lambda_2^5 > -1$ requires that $\gamma D^* + \sqrt{\Delta^*} > -2\bar{w}^*$ which is always satisfied.
   iii. Condition $\lambda_3^5 < 1$ requires that $\gamma D^* - \sqrt{\Delta^*} < 0$ which is always satisfied because $\gamma D^* < (\gamma D^*)^2 + \frac{1}{4}\beta(\beta-\gamma)$.
   iv. Condition $\lambda_3^5 > -1$ requires that $\gamma D^* - \sqrt{\Delta^*} > -2\bar{w}^*$ which is always satisfied because $\alpha > \beta$ given the parametrization of our model.

   Notice that $\beta > \gamma$ implies that $D^* > 0$. In particular, from (14) we know that $D^* = \frac{1}{2(\beta-\gamma)}\left(\sqrt{\delta^2 + \frac{1}{4}(\beta-\gamma)^2} - \delta\right)$ and given that $\delta^2 + \frac{1}{4}(\beta-\gamma)^2 > \delta^2$ the sign of D^* is always equal to the sign of $\beta - \gamma$.

   (b) Eigenvalues $\lambda_{2,3}^5$ are complex conjugate numbers when $\Delta^* < 0$ and thus condition $\beta < \gamma$ is necessary for having complex eigenvalues. If $\beta > \gamma$ and the eigenvalues $\lambda_{2,3}^5$ are complex numbers, the stability

of the internal equilibrium requires that $|\lambda^5_{2,3}| < 1$. This requirement implies the satisfaction of a single condition.

i. Condition $|\lambda^5_2| = |\lambda^5_3| < 1$ requires that $2\gamma\bar{w}^*D^* - \frac{1}{4}\beta(\beta-\gamma) < 0$. Replacing $\bar{w}^*$ and D^* with their definitions from (15) and (14) respectively, yields the new condition $\alpha - \Omega < 4\delta < \alpha + \Omega$ where $\Omega = \frac{(2\gamma-\beta)\sqrt{\gamma(\beta^3-\beta^2\gamma+\alpha^2\gamma)}}{\beta\gamma}$. The term Ω is equal to α if $\beta = \gamma$ but is greater than α if $\beta < \gamma$. This can be shown by calculating the derivative of Ω with respect to β, $\frac{\partial\Omega}{\partial\beta}$, which is negative when $\beta < \gamma$. This is true when $\alpha > \beta, 2\delta$ as is the case given the parametrization of our model. Because Ω is greater than α when $\beta < \gamma$, the stability condition $\alpha - \Omega < 4\delta < \alpha + \Omega$ can be replaced by $0 < 4\delta < 2\alpha$ which is always satisfied given the parametrization of our model. Therefore, when eigenvalues $\lambda^5_{2,3}$ are complex, their modulus is always less than one.

2. Stability conditions derived from the fourth eigenvalue λ^5_4. Eigenvalue λ^5_4 is a real number and the stability of the internal equilibrium requires that $-1 < \lambda^5_4 < 1$. This requirement implies the satisfaction of two conditions:

i. Condition $\lambda^5_4 < 1$ requires that $-\delta - 2D^*(\beta-\gamma) < 0$ which is always satisfied because $\beta - \gamma$ and D^* have the same sign and thus their product is always positive.
ii. Condition $\lambda^5_4 > -1$ requires that $\delta + 2D^*(\beta-\gamma) < 2\bar{w}^*$. Replacing D^* and $\bar{w}^*$ with their definitions from (14) and (15) respectively, yields the new condition $2(\alpha + 2\beta D^*) > \sqrt{\frac{1}{4}(\beta-\gamma)^2 + \delta^2}$. Because $2(\alpha + 2\beta D^*) > 2\alpha - \beta$ and $\frac{1}{2}(\gamma-\beta) + \delta > \sqrt{\frac{1}{4}(\beta-\gamma)^2 + \delta^2}$ the later condition is true when $2\alpha - \beta > \frac{1}{2}(\gamma-\beta) + \delta$ which is always satisfied for the parametrization of our model.

To summarize, internal equilibrium $\mathbf{x}^{*5}$ is unstable (saddle) ($\lambda^5_2 > 1$ but $-1 < \lambda^5_{3,4} < 1$) if $\beta > \gamma$ ($f > \frac{1}{2}c$) but stable ($|\lambda^5_{2,3}| < 1$ and $-1 < \lambda^5_4 < 1$) if $\beta > \gamma$ ($f < \frac{1}{2}c$) (see Table 1 and Fig. 2).

3.3. Dynamics

3.3.1. Infinite population

When viability selection is strong ($f > \frac{1}{2}c$) the dynamics of our system tend towards the fixation of one of the recombination enabling haplotypes ($\mathbf{x}^{*1}$ or $\mathbf{x}^{*4}$) (Figs. 2 and 3.a). In these two corner equilibria, an individual recombination hotspot remains inactive and the genomic recombinational landscape remains unchanged (Fig. 3.a). Furthermore, the PRDM9-like gene does not evolve and remains monomorphic. An unchanging recombinational landscape and a non-evolving PRDM9 gene, are inconsistent with empirical observations on the life history of recombination hotspots controlled by PRDM9 (Ptak et al., 2004, 2005; Winckler et al., 2005; Coop et al., 2008; Myers et al., 2010; Stevison et al., 2015).

When viability selection is weak ($f < \frac{1}{2}c$) and initially all haplotypes are present in the population, the dynamics of our system oscillate towards a polymorphic equilibrium where all haplotypes (enabling and disabling) are present ($\mathbf{x}^{*5}$)(Figs. 2 and 3.b). At this interior equilibrium, an individual recombination hotspot will see its activity reduced but not extinguished, and the genomic recombinational landscape remains unchanged (Fig. 3.b). Furthermore, the PRDM9-like gene does not evolve but remains polymorphic. An unchanging recombinational landscape and a non-evolving PRDM9 gene, are inconsistent with empirical observations (Ptak et al., 2004, 2005; Winckler et al., 2005; Coop et al., 2008; Myers et al., 2010; Stevison et al., 2015).

When viability selection is weak ($f < \frac{1}{2}c$) and initially one haplotype is present while the others are rare mutants, the dynamics of our system oscillate towards a heteroclinic cycle where fixation of one of the recombination enabling haplotypes alternates with fixation of one of the recombination disabling haplotypes ($\ldots\mathbf{x}^{*1} \rightarrow \mathbf{x}^{*2} \rightarrow \mathbf{x}^{*4} \rightarrow \mathbf{x}^{*3} \rightarrow \mathbf{x}^{*1}\ldots$) (Figs. 2 and 3.c). Along this cycle, an individual recombination hotspot will alternate between becoming inactive (die) and becoming active (resurrect) (Fig. 3.c). Therefore, the recombinational landscape becomes highly dynamic (Fig. 3.c). Furthermore, the PRDM9-like gene is evolving fast with selective sweeps that are harder when viability selection is higher within the lower range ($f < \frac{1}{2}c$). A changing recombinational landscape and a rapidly evolving PRDM9 gene, are consistent with empirical observations on the life history of recombination hotspots controlled by PRDM9 (Ptak et al., 2004, 2005; Winckler et al., 2005; Coop et al., 2008; Myers et al., 2010; Stevison et al., 2015).

3.3.2. Finite population

We modeled the cases of an infinite population without recurrent mutation, to better characterize the interaction between selection and conversion. In nature however, the population is finite and mutations are introduced recurrently. We carried out the numerical analysis of a model for a finite population with recurrent mutations at the modifier and target locus to gain insight on the effect of these two variables in our conclusions. The typical dynamics are summarized in Fig. 4. In this figure it can be observed that the cycling remains with an alternation of hotspots and coldspots.

In particular, when viability selection is weak ($f < \frac{1}{2}c$) and initially one of the haplotypes is much more frequent than all the others, the haplotypes fluctuate around the boundary of the simplex, what is the heteroclinic cycle in the corresponding infinite population model ($\mathbf{x}^{*1} \rightarrow \mathbf{x}^{*2} \rightarrow \mathbf{x}^{*4} \rightarrow \mathbf{x}^{*3} \rightarrow \mathbf{x}^{*1}$) (Fig. 4.b). Intuitively, selection and conversion favor the oscillation of haplotypes towards the boundary of the simplex where genetic drift pushes some of them to extinction (Fig. 4.b). Extinction slows down the oscillatory dynamics but does not put an end to them, recurrent mutations re-introduce the missing variation and the system finds itself in the initial conditions that favor the heteroclinic cycle (Fig. 4.b).

When viability selection is weak ($f < \frac{1}{2}c$) and initially all the haplotypes are frequent, the haplotypes fluctuate around the interior of the simplex, what is the polymorphic equilibrium in the infinite population model ($\mathbf{x}^{*5}$) (Fig. 4.a). Intuitively, selection and conversion favor the oscillation of haplotypes towards the interior of the simplex but genetic drift prevents them from settling (Fig. 4.a). Because these oscillations remain far from the boundary the extinction of haplotypes is rarely observed (Fig. 4.a). In the absence of extinction, hotspots and coldspots alternate rapidly. Genetic drift allows the transition from wide oscillations around the boundary to narrower oscillations within the interior and back.

4. Discussion

We find that strong selection (defined as selection bigger than half the conversion) fixes haplotypes which enable double-strand breaks (this translates into individual recombination hotspots that exhibit high activity and do not die over time (Fig. 3.a)). This finding recovers the result of previous models (Boulton et al., 1997; Pineda-Krch and Redfield, 2005; Calabrese, 2007; Peters, 2008). In our model however, weak selection (defined as selection smaller than half the conversion) does not fix any particular

Please cite this article as: F. Úbeda, T.W. Russell and V.A.A. Jansen, PRDM9 and the evolution of recombination hotspots. Theoretical Population Biology (2019), https://doi.org/10.1016/j.tpb.2018.12.005.

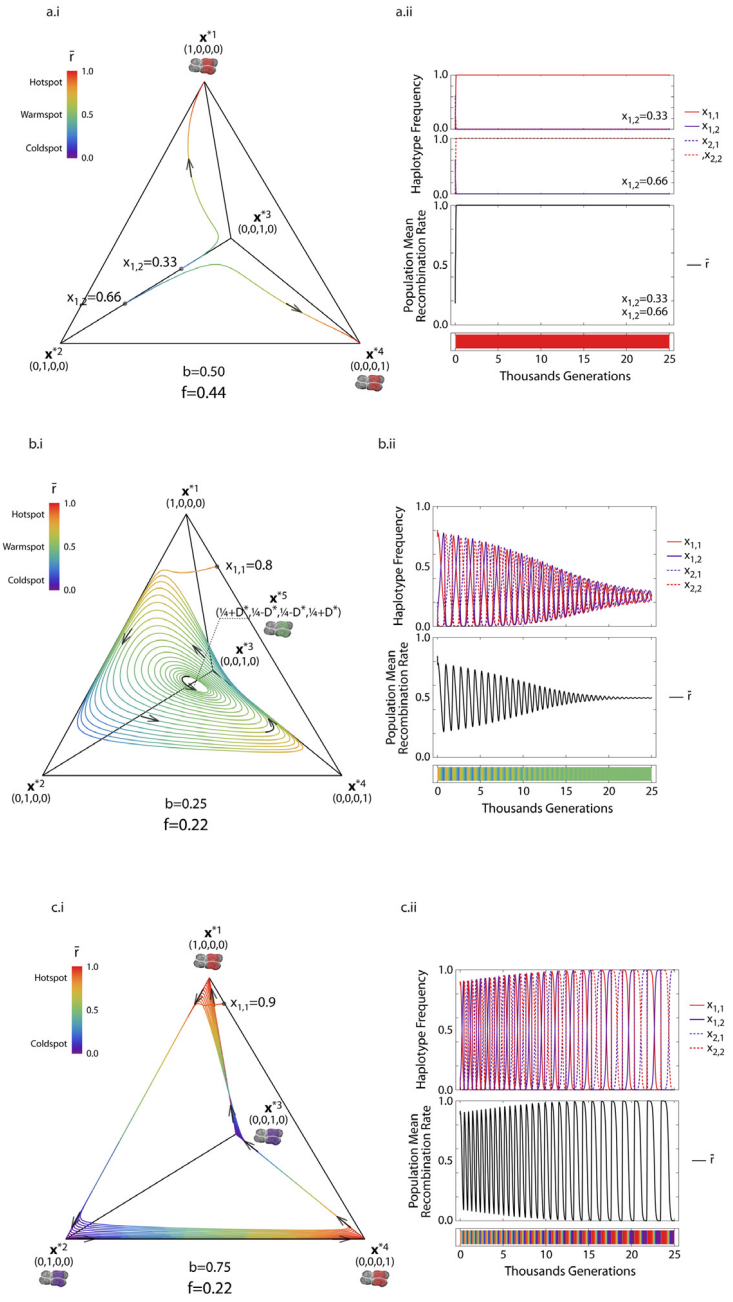

Fig. 3. *Dynamics of the system.* Examples of the three types of dynamics we find in our system. Each panel corresponds to a different combination of parameter values (f, b) and initial conditions $(x^0_{1,1}, x^0_{1,2}, x^0_{2,1}, x^0_{2,2})$, while parameter values r, c remain fixed across panels, in particular $(r, c) = (1, \frac{1}{2})$. Sub-panel (i) depicts the frequency of all haplotypes $(x_{1,1}, x_{1,2}, x_{2,1}, x_{2,2})$ at time t as a point in the three dimensional simplex. Arrows indicate in which direction the dynamics progress as time goes by. The color of the line depicts the population mean recombination activity of the target (see legend). Sub-panel (ii) stacks three plots, namely: each of the haplotype frequencies against generational time, the population mean recombination activity as a line against time, and the population mean recombination activity as heat map against time. Panel (a) corresponds to parameter values $(f, b) = (0.44, 0.50)$ and initial conditions $(0, x^0_{1,2}, 1 - x^0_{1,2}, 0)$ where $x^0_{1,2} = 0.33$ or $x^0_{1,2} = 0.66$. (a.i) shows that when the initial condition is $x^0_{1,2} = 0.33$ the system tends to corner equilibrium $\mathbf{x}^{*1}$. When the initial condition is $x_{1,2} = 0.66$ the system tends to the other stable corner equilibrium $\mathbf{x}^{*4}$. In both cases the target site at equilibrium is a recombination hotspot (target colored). (a.ii) shows that when the initial condition is $x^0_{1,2} = 0.33$ the recombination enabling haplotype $x_{1,1}$ becomes fixed. There are no changes at the modifier locus coding for PRDM9-like proteins. The population mean recombination activity reaches and remains over time at its highest (1). The target site becomes and remains a recombination hotspot over time. Panel (b) corresponds to parameter values $(f, b) = (0.22, 0.25)$ and initial conditions $(x^0_{1,1}, 0, 0, 1 - x_{1,1})$ where $x_{1,1} = 0.80$. (b.i) shows that the system tends to internal equilibrium $\mathbf{x}^{*5}$ where the target site is what we called a recombination warmspot. (b.ii) shows that the frequency of all haplotypes oscillate in their approach to equilibrium where all haplotypes (recombination enabling and disabling) are present. There are oscillations at the locus coding for PRDM9-like proteins in the approach to equilibrium but these changes cease when equilibrium is reached. The population mean recombination activity oscillates between high and low as it approaches an intermediate value (0.5) at equilibrium. The target site oscillates between hot and cold phenotypes as it approaches a warm phenotype at equilibrium. Panel (c) corresponds to parameter values $(f, b) = (0.22, 0.75)$ and initial conditions $(x^0_{1,1}, 0, 0, 1 - x^0_{1,1})$ where $x^0_{1,1} = 0.90$. (c.i) shows that the system tends to the heteroclinic cycle $(\ldots \mathbf{x}^{*1} \to \mathbf{x}^{*2} \to \mathbf{x}^{*4} \to \mathbf{x}^{*3} \to \mathbf{x}^{*1} \ldots)$. (c.ii) shows that the frequency of all haplotypes oscillate in their approach to the heteroclinic cycle where there is an alternation between near fixation of one of the recombination enabling haplotypes and near fixation of one of the recombination disabling haplotypes. There are oscillations at the locus coding for PRDM9-like proteins, oscillations that become increasingly pronounced as the system approaches the heteroclinic cycle. The population mean recombination activity oscillates between high and low, oscillations that become increasingly pronounced as the system approaches the heteroclinic cycle. The target site oscillates between hot and cold phenotypes with it hot and cold character becoming more marked as the system approaches the heteroclinic cycle. (For interpretation of the references to color in this figure legend, the reader is referred to the web version of this article.)

Please cite this article as: F. Úbeda, T.W. Russell and V.A.A. Jansen, PRDM9 and the evolution of recombination hotspots. Theoretical Population Biology (2019), https://doi.org/10.1016/j.tpb.2018.12.005.

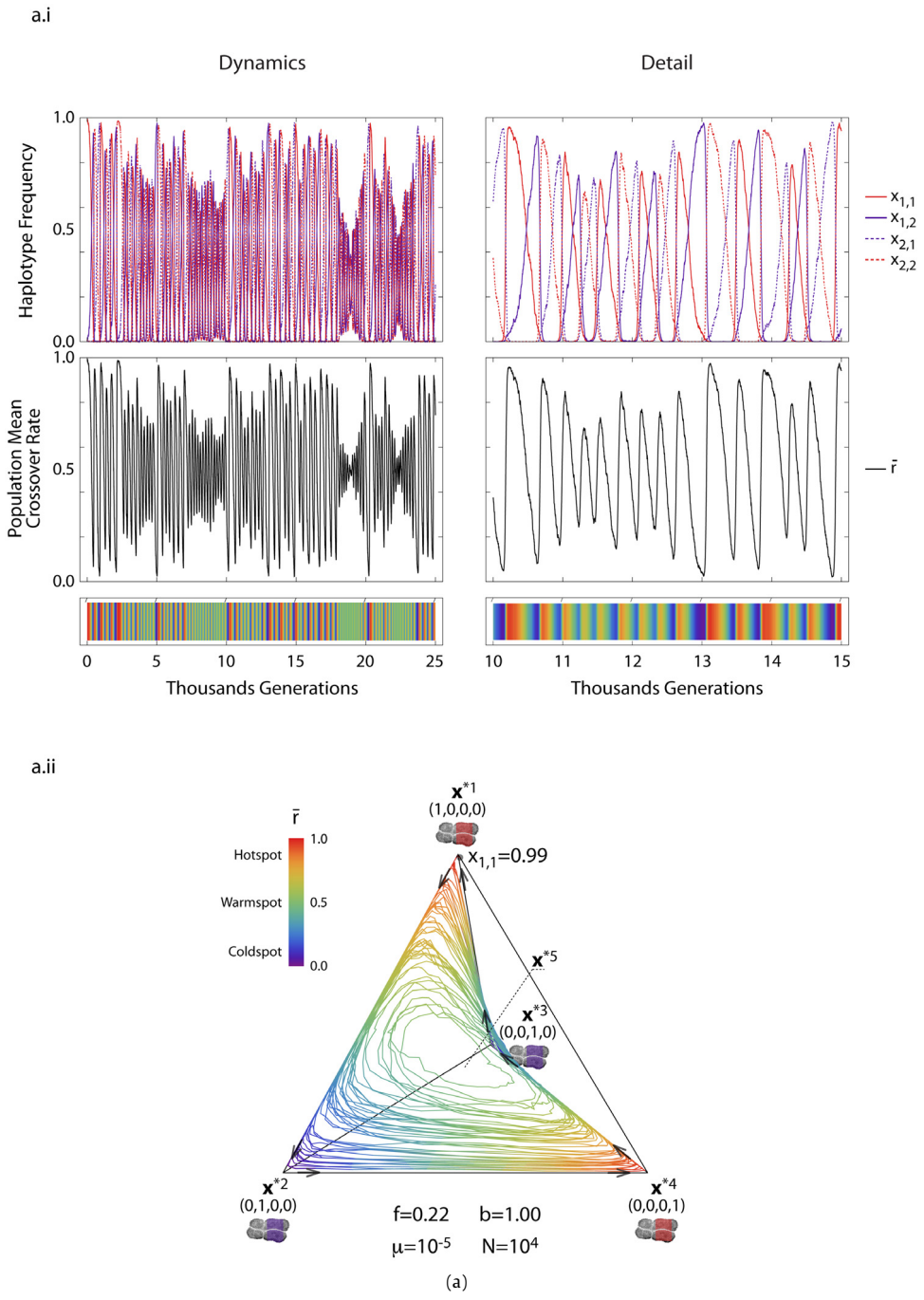

Fig. 4. *Comparison with finite populations.* Examples of the correspondence between dynamics in the infinite and finite population models. Each panel corresponds to a different combination of parameter values (f, b) and (μ, N) where μ is the mutation rate and N is the population size. Parameter values $(r, c) = (1, \frac{1}{2})$ and initial conditions $(x^0_{1,1}, x^0_{1,2}, x^0_{2,1}, x^0_{2,2}) = (0.99, \frac{1}{3}0.01, \frac{1}{3}0.01, \frac{1}{3}0.01)$ remain fixed across panels. Sub panel (i) stacks three plots, namely: each of the haplotype frequencies against generational time, the population mean recombination activity against time, and the population mean recombination activity as a heat map against time. Sub panel (ii) depicts the frequency of all haplotypes $(x_{1,1}, x_{1,2}, x_{2,1}, x_{2,2})$ at time t as a point in the three dimensional simplex. Arrows indicate in which direction the dynamics progress as time goes by. The color of the line depicts the population mean recombination activity of the target site (see legend). Panel (a) corresponds to parameter values $(f, b) = (0.22, 1.00)$ and $(\mu, N) = (10^{-5}, 10^4)$. The target site oscillates between hot and cold phenotypes rapidly and no haplotype becomes fixed. Panel (b) corresponds to parameter values $(f, b) = (0.22, 1.00)$ and $(\mu, N) = (10^{-6}, 10^4)$. The target site oscillates between hot and cold phenotypes slowly and haplotypes often become fixed. (For interpretation of the references to color in this figure legend, the reader is referred to the web version of this article.)

haplotype; it either maintains all haplotypes in constant proportions (which translates into individual recombination hotspots that exhibit moderate activity and do not die (Fig. 3.b)), or the proportion of each haplotype cycles over time (which translates into individual recombination hotspots that exhibit low and high activity, dying and resurrecting in a constant cycle (Fig. 3.c)). These two types of recombination hotspots are novel. An equilibrium that maintains a polymorphism at a PRDM9-like locus and its target has not been described (Latrille et al., 2017). A cycle whereby the same set of alleles at a PRDM9-like locus and its target site rotate has not been described either.

Please cite this article as: F. Úbeda, T.W. Russell and V.A.A. Jansen, PRDM9 and the evolution of recombination hotspots. Theoretical Population Biology (2019), https://doi.org/10.1016/j.tpb.2018.12.005.

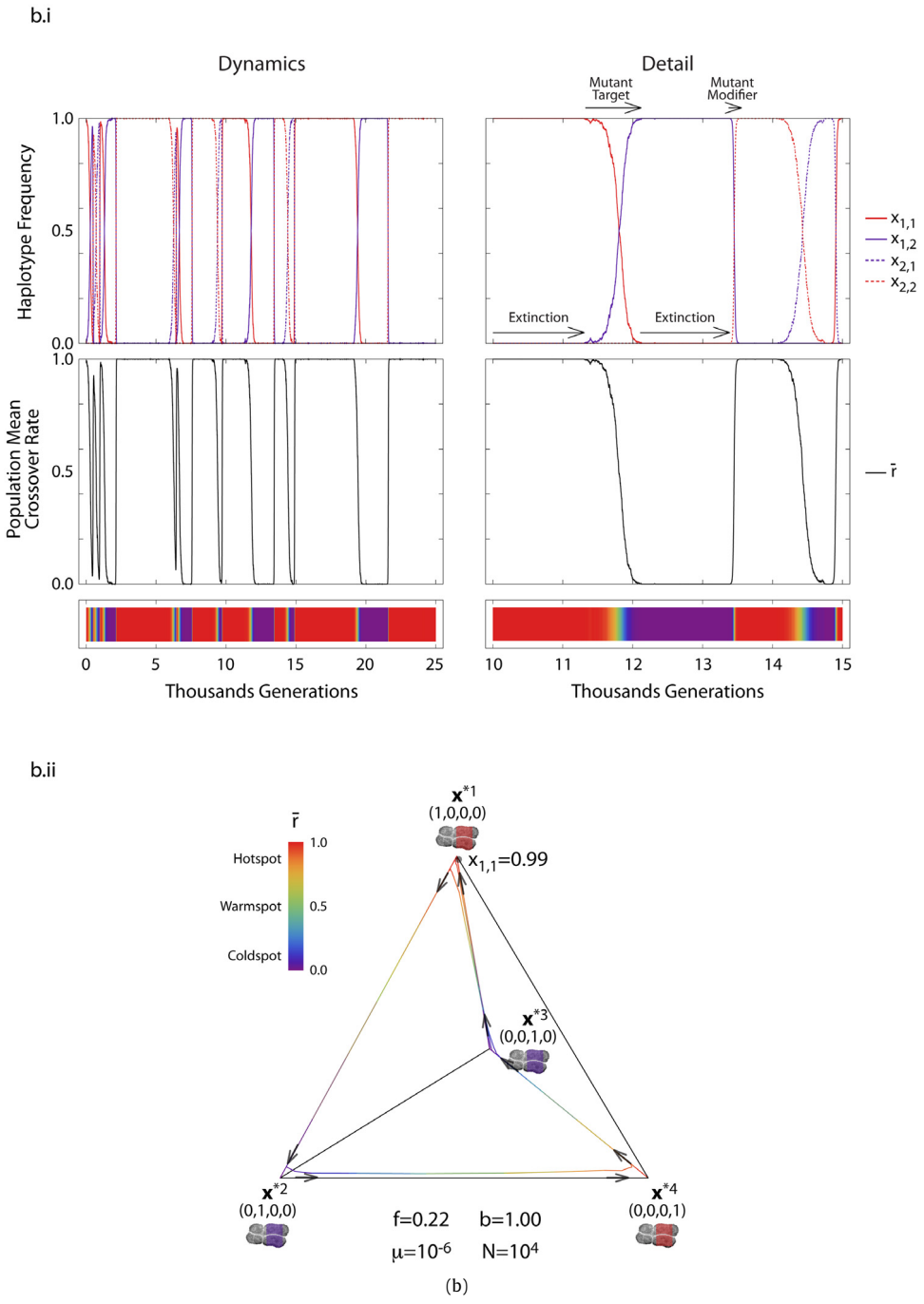

Fig. 4. (*continued*).

It is possible to gain an intuitive interpretation of our formal results if we consider a mutant gene playing a game against another gene from a gamete pool in a diploid individual. A mutant gene can play four strategies ($A_1B_1, A_1B_2, A_2B_1, A_2B_2$) and the gamete pool is formed by the same four strategies. The payoff of each gene interaction is summarized in the payoff matrix provided in Fig. 5 and is determined by the individual fitness cost of not experiencing a DSB ($F_k = f > 0$), the allelic conversion benefit (or cost) of not experiencing (or experiencing) a DSB ($C_b = \frac{1}{2}c > 0$), and a recombination shuffling factor that determines which alleles benefit from conversion in double heterozygotes ($R_s = f(r) > 0$). Let us start by considering a population almost fixed for a recombination enabling haplotype A_1B_1. If fitness cost is greater than conversion benefit ($F_k > C_b$), our resident population of A_1B_1 cannot be invaded by any alternative strategy ($1 > 1 - \frac{1}{2}F_k + \frac{1}{2}C_b$; Fig. 5.a). Therefore strong selection favors highly active permanent recombination hotspots (Fig. 3.a). If fitness cost is lower than conversion benefit ($F_k < C_b$; Fig. 5.b), our resident population of A_1B_1 can be invaded by the rare mutant A_1B_2 ($1 - \frac{1}{2}F_k + \frac{1}{2}C_b > 1 - \frac{1}{2}F_k + R_s > 1$ when $C_b > 2R_s$; Fig. 5.b) as it gains a transmission advantage that more than compensates for its fitness cost; once A_1B_2 becomes the resident haplotype, it can be invaded by rare mutant $A_2B_2(1 - \frac{1}{2}F_k > 1 - F_k$; Fig. 5.b) as it gains a fitness benefit and does not suffer a transmission disadvantage, once A_2B_2 becomes the resident it can be invaded by rare mutant $A_2B_1(1 - \frac{1}{2}F_k + \frac{1}{2}C_b > 1$; Fig. 5.b), and once A_2B_1 becomes the resident it can be invaded by rare mutant A_1B_1

Please cite this article as: F. Úbeda, T.W. Russell and V.A.A. Jansen, PRDM9 and the evolution of recombination hotspots. Theoretical Population Biology (2019), https://doi.org/10.1016/j.tpb.2018.12.005.

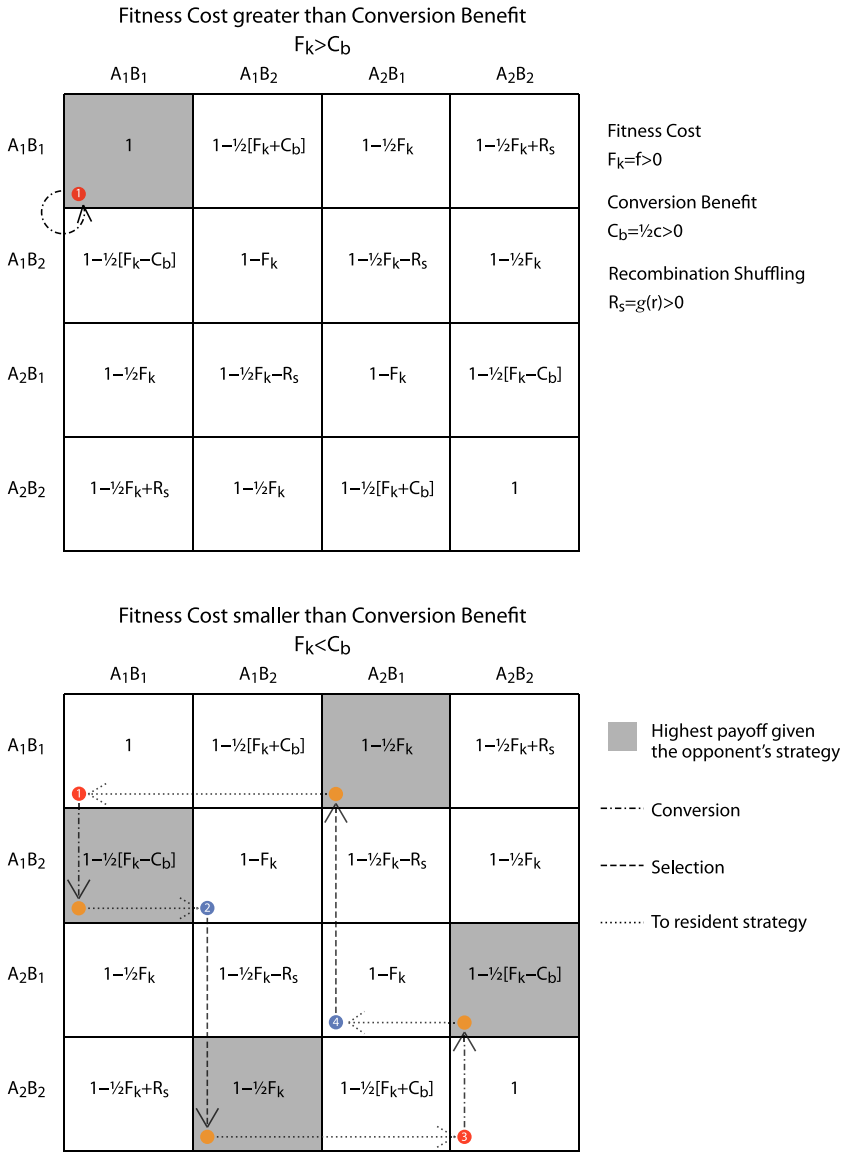

Fig. 5. *Evolutionary game.* Payoff matrix of a game played by each haplotype against a haplotype pool. The payoff is determined by the possibility of a diploid genotype containing that haplotype experiencing a fitness cost (F_k) due to the absence of a double-strand break , a conversion benefit (C_b) – or conversion cost ($-C_b$) – due to the conversion of the opponent's haplotype into the player's haplotype — or the conversion of the player's haplotype into the opponent's haplotype, and a reshuffling benefit or cost due to the generation of the player's or the opponent's haplotype due to the formation of new combinations of alleles. In the first matrix we assume that the fitness cost is greater than the conversion benefit ($F_k > C_b$). Starting with a population fixed for haplotype A_1B_1, A_1B_1 is the mutant strategy that gives the highest payoff (in gray in the matrix). No mutant haplotype can invade and A_1B_1 is the only evolutionary stable strategy. In the second matrix we assume that the fitness cost is smaller than the conversion benefit ($F_k < C_b$). Starting with a population fixed for haplotype A_1B_1, A_1B_2 is the mutant strategy that gives the highest payoff (in gray in the matrix) and should take over the population. When A_1B_2 has become the resident strategy, A_2B_2 is the mutant strategy that gives the highest payoff (in gray in the matrix) and should take over the population. Using the same logic becomes obvious that in this second game there is no pure evolutionary stable strategy but a continuous cycling of strategies.

$(1-\frac{1}{2}F_k > 1-F_k$; Fig. 5.b) thus completing a recurrent cycle. Therefore weak selection and abundance of only one haplotype, can favor recombination hotspots that alternate between low and high activity; dying and resurrecting in cyclic succession (Fig. 3.c). When all haplotypes are frequent in the initial population, the abundance of double heterozygotes results in the shuffling of the transmission advantage between different haplotypes. Depending on intensity of the shuffling. either the previous cycle is maintained or the best strategy becomes to play a fixed proportion of each strategy. Therefore weak selection and abundance of all haplotypes, can favor recombination hotspots that exhibit moderate activity and do not die (Fig. 3.b), providing an intuitive interpretation of our analysis.

These findings provide a novel solution to the recombination hotspots paradox (Boulton et al., 1997). In the prevailing explanation (the Red Queen theory), individual recombination hotspots die and are saved from extinction in the genome by the birth of new recombination hotspots at new target sites in the genome (Myers et al., 2010; Baudat et al., 2010; Úbeda and Wilkins, 2011). Viability selection favors mutant PRDM9 alleles that bind new target sites (Úbeda and Wilkins, 2011). In our model, viability selection does not prevent the death of individual recombination hotspots but saves them from extinction in the genome by driving their resurrection in homozygous targets where the effect of conversion is negligible (Figs. 3, 4). Selection favors mutant PRDM9 alleles that bind the alternative target allele within the same target site. Both theories succeed in explaining the life history of recombination hotspots characterized by: i. the death of individual recombination hotspots not leading to the their extinction in the genome (notice however that in principle the Red Queen theory would require a never ending supply of targets to prevent the extinction); ii. rapid

change of the recombinational landscape; iii. rapid evolution of PRDM9. In our model however, this life history is explained by the bottom range of viability selection parameters which seems more plausible from an empirical perspective). Furthermore, our model makes novel predictions that the Red Queen (at least in its present formulation) does not. In particular, our model predicts that: i. the molecular signature near recombination hotspots should be the one of multiple recurrent events of high crossover activity as opposed to a single even of high crossover activity; ii. viability selection can maintain polymorphisms in PRDM9 (as opposed to Latrille et al., 2017); iii. the same genetic architecture under the same selection regime can result in two different families of recombination hotspots, one family with alternation of high and low activity and another family with constant intermediate activity.

For the purpose of characterizing the interplay between selection and conversion on the evolution of recombination hotspots, our model makes a series of simplifying assumptions provided in the Methods section. Many of these assumptions are standard in population genetics models and relaxing all of them is beyond the scope of this manuscript. However, relaxing some of them will help us to better understand the empirical relevance of our model. In particular, we discuss the implications of considering multiple alleles and target loci and a finite population.

Our analysis assumes one modifier and one target locus with two alleles in each locus. In humans there are multiple alleles segregating at locus PRDM9 and multiple alleles at each of many target sites. We numerically explored how our conclusions change when either the number of alleles in each locus is increased or the number of target loci is increased. The dynamics in a model with three alleles remains very similar. If viability selection is weaker than gene conversion, the cycling is still observed although the fluctuations become irregular and unpredictable (chaotic). This is consistent with intuition, as a modifier converts its specific target, it amplifies the frequency of any of the remaining targets. If one of the remaining targets attains a sufficiently high frequency, it will then allow selection on the accompanying modifier. The dynamics in a model with two targets also remains very similar. If viability selection is weaker than gene conversion, the cycling is still observed and the fluctuations between different targets can be either synchronized or not. Multiple targets allows selection on modifiers that match one of both targets. More realistic models would require considering larger number of alleles and target sites.

Our analysis assumes an infinite population without recurrent mutations, however populations in nature are finite and mutations are recurrent. We numerically explored how our conclusions change when we consider a finite population with recurrent mutations. If viability selection is weaker than gene conversion, the cycling is still observed although the cycles now drift in amplitude due to the stochastic effects. The dynamics may spend more time in the vicinity of the interior of the simplex (the interior equilibrium in the infinite population), where genetic drift rarely pushes any allele to extinction (Fig. 4.a). The dynamics may spend more time in the vicinity of the boundary of the simplex (the heteroclinic cycle in the infinite population), where genetic drift often pushes some of alleles to extinction and that the dynamics become stuck. Once a suitable mutation occurs the dynamics continue fluctuating (Fig. 4.b). Stochasticity allows transitions from oscillations mostly around the interior to mostly around the boundary.

Relaxing some of our assumptions in our model, suggests that in a finite population with multiple alleles and target locus our main result holds; individual hotspots will die but they will resurrect later in evolutionary time, thus precluding their extinction from the genome in the long term. Population size, mutation rates, and number of targets will affect the turnover rate of recombination hotspots but not the qualitative behavior of the selection conversion dynamics mediated by haplotype matching. This suggests that our solution to the recombination hotspot paradox is robust although larger numbers of target sites and their interplay with population size need to be modeled before a conclusion can be reached.

Acknowledgments

[FU] thanks Amaya and Emma Úbeda for their continuous support.

Author contributions

[FU] conceived the research, [FU] formulated the model, [TR] and [VJ] analyzed the model with feedback from [FU], [TR] carried out the numerical analysis, and [FU] wrote the paper with feedback from [TR] and [VJ].

Appendix A. Supplementary data

Supplementary material related to this article can be found online at https://doi.org/10.1016/j.tpb.2018.12.005.

References

Alves, I., Houle, A.A., Hussin, J.G., Awadalla, P., 2017. The impact of recombination on human mutation load and disease. Philos. Trans. R. Soc. B 372 (1736), 20160465.
Baker, B.S., Carpenter, A.T., Esposito, M.S., Esposito, R.E., Sandler, L., 1976. The genetic control of meiosis. Annu. Rev. Genet. 10 (1), 53–134.
Baudat, F., Buard, J., Grey, C., Fledel-Alon, A., Ober, C., Przeworski, M., Coop, G., De Massy, B., 2010. Prdm9 is a major determinant of meiotic recombination hotspots in humans and mice. Science 327 (5967), 836–840.
Baudat, F., Imai, Y., De Massy, B., 2013. Meiotic recombination in mammals: localization and regulation. Nature Rev. Genet. 14 (11), 794.
Boulton, A., Myers, R.S., Redfield, R.J., 1997. The hotspot conversion paradox and the evolution of meiotic recombination. Proc. Natl. Acad. Sci. 94 (15), 8058–8063.
Brick, K., Smagulova, F., Khil, P., Camerini-Otero, R.D., Petukhova, G.V., 2012. Genetic recombination is directed away from functional genomic elements in mice. Nature 485 (7400), 642.
Bürger, R., 2000. The Mathematical Theory of Selection, Recombination, and Mutation. John Wiley & Sons.
Calabrese, P., 2007. A population genetics model with recombination hotspots that are heterogeneous across the population. Proc. Natl. Acad. Sci. 104 (11), 4748–4752.
Coop, G., Myers, S.R., 2007. Live hot, die young: transmission distortion in recombination hotspots. PLoS Genet. 3 (3), e35.
Coop, G., Wen, X., Ober, C., Pritchard, J.K., Przeworski, M., 2008. High-resolution mapping of crossovers reveals extensive variation in fine-scale recombination patterns among humans. science 319 (5868), 1395–1398.
Hassold, T., Hunt, P., 2001. To err (meiotically) is human: the genesis of human aneuploidy. Nature Rev. Genet. 2 (4), 280.
Hassold, T., Sherman, S., Hunt, P., 2000. Counting cross-overs: characterizing meiotic recombination in mammals. Hum. Mol. Genet. 9 (16), 2409–2419.
Hey, J., 2004. What's so hot about recombination hotspots? PLoS Biol. 2 (6), e190.
Karlin, S., Feldman, M.W., et al., 1970. Linkage and selection: two locus symmetric viability model. Theor. Popul. Biol. 1 (1), 39–71.
Koehler, K.E., Hawley, R.S., Sherman, S., Hassold, T., 1996. Recombination and nondisjunction in humans and flies. Hum. Mol. Genet. 5 (Supplement_1), 1495–1504.
Latrille, T., Duret, L., Lartillot, N., 2017. The red queen model of recombination hotspot evolution: a theoretical investigation. Philos. Trans. R. Soc. B 372 (1736), 20160463.
Lesecque, Y., Glémin, S., Lartillot, N., Mouchiroud, D., Duret, L., 2014. The red queen model of recombination hotspots evolution in the light of archaic and modern human genomes. PLoS Genet. 10 (11), e1004790.
Lichten, M., Goldman, A.S., 1995. Meiotic recombination hotspots. Annu. Rev. Genet. 29 (1), 423–444.
Louis, E.J., Borts, R.H., 2003. Meiotic recombination: too much of a good thing? Curr. Biol. 13 (24), R953–R955.
Myers, S., Bottolo, L., Freeman, C., McVean, G., Donnelly, P., 2005. A fine-scale map of recombination rates and hotspots across the human genome. Science 310 (5746), 321–324.
Myers, S., Bowden, R., Tumian, A., Bontrop, R.E., Freeman, C., MacFie, T.S., McVean, G., Donnelly, P., 2010. Drive against hotspot motifs in primates implicates the PRDM9 gene in meiotic recombination. Science 327 (5967), 876–879.
Paigen, K., Petkov, P., 2010. Mammalian recombination hot spots: properties, control and evolution. Nature Rev. Genet. 11 (3), 221.

Peters, A., 2008. A combination of cis and trans control can solve the hotspot conversion paradox. Genetics.

Petes, T.D., 2001. Meiotic recombination hot spots and cold spots. Nature Rev. Genet. 2 (5), 360.

Pineda-Krch, M., Redfield, R., 2005. Persistence and loss of meiotic recombination hotspots. Genetics.

Ptak, S.E., Hinds, D.A., Koehler, K., Nickel, B., Patil, N., Ballinger, D.G., Przeworski, M., Frazer, K.A., Pääbo, S., 2005. Fine-scale recombination patterns differ between chimpanzees and humans. Nat. Genet. 37 (4), 429.

Ptak, S.E., Roeder, A.D., Stephens, M., Gilad, Y., Pääbo, S., Przeworski, M., 2004. Absence of the tap2 human recombination hotspot in chimpanzees. PLoS Biol. 2 (6), e155.

Rosenberg, N.A., Huang, L., Jewett, E.M., Szpiech, Z.A., Jankovic, I., Boehnke, M., 2010. Genome-wide association studies in diverse populations. Nature Rev. Genet. 11 (5), 356.

Russell, T.W., Russell, M.J., Úbeda, F., Jansen, V.A.A., 2019. Stable Cycling in Quasi-Linkage Equilibrium: Fluctuating Dynamic under Gene Conversion and Selection. Submitted for publication.

Ségurel, L., Leffler, E.M., Przeworski, M., 2011. The case of the fickle fingers: how the prdm9 zinc finger protein specifies meiotic recombination hotspots in humans. PLoS Biol. 9 (12), e1001211.

Stevison, L.S., Woerner, A.E., Kidd, J.M., Kelley, J.L., Veeramah, K.R., McManus, K.F., Project, G.A.G., Bustamante, C.D., Hammer, M.F., Wall, J.D., 2015. The time scale of recombination rate evolution in great apes. Mol. Biol. Evol. 33 (4), 928–945.

Sun, H., Treco, D., Szostak, J.W., 1991. Extensive 3'-overhanging, single-stranded DNA associated with the meiosis-specific double-strand breaks at the ARG4 recombination initiation site. Cell 64 (6), 1155–1161.

Szostak, J.W., Orr-Weaver, T.L., Rothstein, R.J., Stahl, F.W., 1983. The double-strand-break repair model for recombination. Cell 33 (1), 25–35.

Úbeda, F., Wilkins, J., 2011. The red queen theory of recombination hotspots. J. Evol. Biol. 24 (3), 541–553.

Winckler, W., Myers, S.R., Richter, D.J., Onofrio, R.C., McDonald, G.J., Bontrop, R.E., McVean, G.A., Gabriel, S.B., Reich, D., Donnelly, P., et al., 2005. Comparison of fine-scale recombination rates in humans and chimpanzees. Science 308 (5718), 107–111.

Wright, S., 1969. Evolution and the Genetics of Populations: Vol. 2. The Theory of Gene Frequencies.

Please cite this article as: F. Úbeda, T.W. Russell and V.A.A. Jansen, PRDM9 and the evolution of recombination hotspots. Theoretical Population Biology (2019), https://doi.org/10.1016/j.tpb.2018.12.005.